

Applications of the Density Matrix Renormalization Group to Exchange-Coupled Transition Metal Systems



Vera Krewald and Dimitrios A. Pantazis

Abstract Transition metal complexes containing magnetically interacting open-shell ions are important for diverse areas of molecular science. The reliable prediction and computational analysis of their electronic structure and magnetic properties, either in qualitative or quantitative terms, remain a central challenge for theoretical chemistry. The use of multireference methods is in principle the ideal approach to the inherently multireference problem of exchange coupling in oligonuclear transition metal complexes; however, the applicability of such methods has been severely restricted due to their computational cost. In recent years, the introduction of the density matrix renormalization group (DMRG) to quantum chemistry has enabled the multireference treatment of chemical problems with previously unattainable numbers of active electrons and orbitals. This development also paved the way for the first-principles multireference treatment of magnetic properties in the case of exchange-coupled transition metal systems. Here, the first detailed applications of DMRG-based methods to exchange-coupled systems are reviewed and the lessons learned so far regarding the applicability, apparent limitations, and future promise of this approach are discussed.

1 Introduction

Systems with multiple interacting open-shell transition metal ions are encountered in areas of science as diverse as active sites of metalloenzymes and synthetic molecular complexes or solid-state inorganic systems. The defining feature of these systems

V. Krewald

Fachbereich Chemie, Technische Universität Darmstadt, Alarich-Weiss-Straße 4,
64287 Darmstadt, Germany

e-mail: krewald@chemie.tu-darmstadt.de

D. A. Pantazis (✉)

Max-Planck-Institut Für Kohlenforschung, Kaiser-Wilhelm-Platz 1,
45470 Mülheim an der Ruhr, Germany

e-mail: dimitrios.pantazis@kofo.mpg.de

© Springer Nature Switzerland AG 2019

E. Broclawik et al. (eds.), *Transition Metals in Coordination Environments*,
Challenges and Advances in Computational Chemistry and Physics 29,
https://doi.org/10.1007/978-3-030-11714-6_4

is that the interaction between the spin of unpaired electrons, often called magnetic or exchange coupling, gives rise to unique magnetic and spectroscopic properties that could not arise from the isolated transition metal centers. The magnitude and the nature of the coupling, for example, ferromagnetic or antiferromagnetic, have profound impact on the properties and reactivity of these systems. One of the great challenges for quantum chemistry is to understand these interactions in the context of electronic structure theory, connect the fundamental description with the phenomenological models often employed in the analysis of experiments, and finally predict the relevant parameters that describe the properties of such exchange-coupled systems with high accuracy and reliability.

The spin states associated with this situation (magnetic levels) typically arise from a single electronic configuration, but can be formally described only with linear combinations of multiple determinants. In contrast to spin states that correspond to distinct configurations of *d* electrons, such as, a low-spin and high-spin configuration of a transition metal ion, the magnetic levels of an exchange-coupled system span a narrow energy range of a few tens or hundreds of wavenumbers [1]. The demands imposed on quantum chemical calculations that target magnetically coupled states are therefore of the order of a wavenumber, and hence much higher than the usual definitions of “chemical accuracy” related to the prediction of common thermodynamic properties ($1 \text{ cm}^{-1} = 0.00286 \text{ kcal/mol} = 0.01196 \text{ kJ/mol}$, or $1 \text{ kJ/mol} = 0.239 \text{ kcal/mol} = 83.593 \text{ cm}^{-1}$). The computational method of choice must therefore be able to predict the energies of all spin states of the magnetically coupled system equally well and converge them to the same accuracy.

Several quantum chemical approaches have been proposed to achieve qualitative and quantitative descriptions of magnetic coupling in molecular complexes with open-shell transition metal ions [2–6]. Density functional theory (DFT) based on the broken-symmetry approach [7–10] has been used for a wide range of systems over several decades with varying levels of success. However, the problem of exchange coupling is inherently a multireference problem that should be formally treated with multireference methods. These have also a long history in the field of exchange-coupled transition metal systems, but their applicability has been severely limited to small dinuclear systems with very few unpaired electrons, for example, Cu(II) dimers [2, 11]. This is due to the steeply increasing cost of multireference calculations for problems with more than a few electrons in a few orbitals. The key challenge of how to enable treatment of large active spaces, for example, in complete active space self-consistent field (CASSCF) calculations, is of direct relevance for the treatment of exchange-coupled transition metal systems, where the presence of more than two metal ions, of many unpaired electrons, or the necessity to include electrons and orbitals of bridging ligands in the active space quickly renders such calculations entirely impossible.

The focus of this chapter is on a method that was introduced relatively recently to the theoretical chemistry community, the density matrix renormalization group (DMRG) [12, 13]. From the point of view of applied quantum chemistry, DMRG can be considered as a method that enables the use of large active spaces in multireference calculations. It has already been employed in configuration interaction

calculations, DMRG-CI, as well as in calculations involving orbital optimization, DMRG-SCF, to a range of chemical questions (for example [14–17]). DMRG-SCF has been reported for dinuclear and even tetranuclear complexes with open-shell transition metals [18–21], although these studies have focused on specific electronic states of the systems of interest without addressing explicitly the problem of exchange coupling. It is important to stress this point because the methodological and technical requirements for the application of DMRG-based approaches are neither obvious nor necessarily transferrable from other wavefunction-based approaches. At the time of this writing, very few studies have used DMRG to predict the relative energies of spin states that arise from magnetic coupling in transition metal clusters. Our aim is to review two of these very first case studies [22, 23] in order to understand the technical and methodological challenges encountered in applications of DMRG to problems of magnetic coupling, as well as to highlight the emerging opportunities that DMRG brings for the computational treatment of these systems. The point of view adopted here is of application-oriented quantum chemistry; the reader interested in the theoretical foundations of the methods and in current theoretical developments is directed to existing excellent reviews [24–27].

2 Theoretical Treatment of Exchange Coupling

The phenomenological Heisenberg–Dirac–van Vleck (HDvV) Hamiltonian is typically used to model the energy spacing between the magnetic levels in terms of pairwise exchange coupling constants and additional parameters. For two centers with spins S_A and S_B , the simplest form of the HDvV Hamiltonian can be written as:

$$\hat{H}_{\text{HDvV}} = -2JS_A S_B$$

This is often the leading or the only term considered and the exchange coupling constant J determines the nature of the fictitious magnetic interaction, ferromagnetic for positive, and antiferromagnetic for negative values. In this case, the energies of adjacent energy levels with total coupled spin $S = S_A + S_B, S_A + S_B - 1, \dots, |S_A - S_B|$ conform to the Landé interval rule:

$$E(S) - E(S - 1) = -2JS$$

Additional terms are used in order to model deviations from isotropic behavior. These include, for example, the biquadratic term $j(\mathbf{S}_A \cdot \mathbf{S}_B)^2$, double exchange $\pm B(S + 1/2)$ in the case of some mixed-valence systems, zero-field splitting terms for total $S \geq 1$, etc. The interested reader is referred to the landmark book of Bencini and Gatteschi for in-depth discussions [28]. Experimental data on the lowest energy levels, such as those derived from magnetic susceptibility measurements,

electron paramagnetic resonance spectroscopy, or polarized neutron diffraction, are fitted with such a phenomenological Hamiltonian as appropriate to the chemical system at hand, yielding numerical values for the terms introduced above. In order to make the fitting problem tractable and reasonably defined, simplifying assumptions are often made regarding the relative magnitudes of particular coupling constants and the magnetic topology of a compound. Importantly, for a sufficiently complex system the fitting cannot be unique, not even if the Hamiltonian is restricted to a single term [29]. Instead of treating the quantities that appear in the HDvV Hamiltonian as merely numerical parameters to be fitted, quantum chemistry attempts to assign physical meaning to these parameters by connecting them with fundamental aspects of the electronic structure, thus enabling both interpretation and prediction by first principles.

The magnetic coupling problem is inherently a multireference problem: Even if the ground state of an exchange-coupled system is described by a single electronic configuration, that is, a unique distribution of electrons among a set of metal-based orbitals, the resulting spin states are multideterminantal. Nevertheless, the use of approximate treatments based on single-determinant methods has a long tradition in computational studies of exchange-coupled transition metal systems. With the exception of approaches that allow local spins to be non-collinear, single-reference treatments are mostly restricted to broken-symmetry DFT (BS-DFT). A Kohn–Sham determinant can formally represent only the magnetically coupled state with maximum total spin multiplicity (e.g., for a dinuclear complex with local spins \mathbf{S}_A and \mathbf{S}_B , $S_{\max} = S_A + S_B$), referred to as the high-spin (HS) solution. For all other rungs of the spin ladder with $S < S_{\max}$, more than one determinant is required. The broken-symmetry (BS) formalism was introduced to circumvent this problem [6–8, 30, 31]. Here, an unrestricted determinant is constructed with an M_S value equal to that of the antiferromagnetically coupled state ($S_{\min} = |S_A - S_B|$). In the BS determinant, the singly occupied orbitals of opposite spin (“magnetic orbitals”) are allowed to localize at the spin centers while retaining overlap “tails” [7, 32, 33]. The BS determinant is not a spin eigenfunction, and hence, it has no defined spin quantum number S ; it can be seen as a weighted mixture [34] of all spin states that contain magnetic sublevels with the same magnetic quantum number M_S .

A central question is how to interpret the energy of the BS solution. Several mapping procedures have been proposed and they all use the energy difference between the HS and BS determinants, relying on assumptions regarding a valid form of a phenomenological Hamiltonian, focusing chiefly on isotropic bilinear exchange [7, 10, 35, 36]. A popular expression for two-spin systems was proposed by Yamaguchi, who used the total spin angular momentum expectation values of the HS and BS determinants to provide a consistent description for weakly to strongly coupled systems [10, 36]:

$$J = -\frac{E_{\text{HS}} - E_{\text{BS}}}{\langle S^2 \rangle_{\text{HS}} - \langle S^2 \rangle_{\text{BS}}}$$

Having obtained a value for the exchange coupling constant J , the spin-state ordering and the relative energies of all rungs of the spin ladder are deduced through the HDvV Hamiltonian. The generalization to oligonuclear systems with N spin centers is straightforward but of rapidly increasing complexity as one needs to determine the values of up to $N(N - 1)/2$ pairwise exchange coupling constants J_{ij} . These are accessible through the computation of up to 2^{N-1} distinct broken-symmetry determinants. For more than three non-symmetry-related spin centers, the number of possible BS determinants can exceed the number of pairwise exchange coupling constants. This leads to an overdetermined system of equations, which can be solved via singular value decomposition [37] to obtain a set of exchange coupling constants J_{ij} that is unique in the least-squares sense [29, 38]. It is noted that a generalized spin projection method has also been introduced for oligonuclear systems [39].

Despite the extensive use of BS-DFT [40–52], the approach has significant limitations. In terms of energetics, the application of the method suffers by the pronounced sensitivity on the density functional and relies on empirical benchmarking against experimental data [4, 5, 53–55]. Although the charge density of the system described by the broken-symmetry determinant is often reliable, the spin density of any state other than the high-spin solution is qualitatively incorrect [4, 56]. The intermediate spin states are not accessible at all by the broken-symmetry formalism; only their energies relative to the HS or BS energy can be predicted, and this only indirectly [4]. This necessitates the use of approximate spin projection methods for predicting spin-dependent properties. Moreover, the interpretation of magnetic coupling based on BS determinants is often limited to qualitative analysis or visualization of magnetic orbitals via the corresponding orbital transformation of Amos and Hall [33, 57] which is not obviously extendable beyond dinuclear species [47].

Multireference wavefunction-based calculations present a distinct quantum chemical alternative, because they offer an opposite approach to the problem. Instead of trying to approximate the HDvV solution space based on a much more limited and approximate number of single-determinant solutions, one can work directly with the (approximate) solutions of the Schrödinger equation. In this case, no assumptions are required regarding the form and the terms of a phenomenological HDvV Hamiltonian, and hence the problem can be approached from the opposite direction than that represented by BS-DFT. CI (if only the coefficients of distinct configuration state functions are optimized) and CASSCF [58, 59] (if the orbitals are also optimized) are examples of multireference methods by which all individual spin states of the magnetically coupled system can be accessed directly.

To describe a magnetically coupled system at the very least, the magnetic orbitals have to be considered in the construction of a minimal active space. A common expansion of the active space in systems with first-row transition metal ions is to include unoccupied d orbitals. The so-called double shell, $3d'$ or $4d$ orbitals are important for an adequate description of radial electron correlation [60, 61]. Considering the Anderson model of superexchange, by which bridging ligands mediate the transfer of spin between the individual spin sites, it is obvious that to describe magnetically coupled systems larger active spaces are needed than in cases that are dominated by the local properties of an individual transition metal ion. A logical extension of the

minimal valence space is thus to include orbitals of the bridging ligands [2], which turns on various types of charge-transfer excitations that contribute to charge and spin polarization effects and adjust the weight of neutral and ionic determinants to better describe the low-energy region of the spin ladder for the exchange-coupled system.

The total size of the active space is commonly abbreviated with the $(N_{\text{electrons}}, N_{\text{orbitals}})$ notation, e.g., (12, 10) denotes an active space with 12 electrons in 10 orbitals. Given that the upper limit for an active space size that can be practically treated with CASSCF is around 16–18 orbitals, the method may be inapplicable even for relatively simple dinuclear exchange-coupled systems. The selection of orbitals that should enter the active space in addition to the magnetic orbitals, the details of orbital preparation and optimization, the number of states targeted, and other technical choices are crucial factors for the design and ultimately for the success of a computational study. Still, a CASSCF treatment does not afford quantitative predictions, and may even fail qualitatively, because despite the formally correct multiterminantal description of the states, dynamic electron correlation is absent. Some of this may be recovered by applying second-order perturbation theory to the CASSCF wavefunction (complete active space second-order perturbation theory, CASPT2 [62, 63], or N -electron valence second-order perturbation theory, NEVPT2 [64, 65]). In contrast to these perturbational methods, difference-dedicated configuration interaction (DDCI) is a variational approach, in which particular classes of CT-excitations are included explicitly in the wavefunction [2, 11, 66–71]. DDCI was suggested to have considerably better performance and robustness for exchange-coupled systems over CASPT2 [72], but its applicability remains severely restricted to minimalistic problems because of its high computational cost.

Although by no means the only issue that has to be addressed, increasing the size of the active space appears as the major obstacle to applications of multiconfigurational SCF methods in exchange-coupled transition metal systems. One way of dealing with this problem has been to use partitioning or truncation schemes, as represented for example by the restricted active space (RAS) [73, 74], the generalized active space (GAS) [75], and the split GAS [76, 77] approaches. Alternatively, the active space limitations are attacked through novel algorithmic approaches, such as the stochastic full configuration interaction quantum Monte Carlo (FCIQMC) [78, 79] technique, and the DMRG approach that is the subject of this chapter.

3 The Density Matrix Renormalization Group Approach

The DMRG algorithm, its implementation, and the extraction of (chemical) observables have been discussed in many papers and reviews [12, 13, 25, 26, 80–88]. Its importance and relevance in particular to inorganic complexes lies in enabling the description of large active spaces in CASCI and CASSCF calculations. Here, we present a qualitative description of the fundamental concepts and highlight practical considerations for the application to open-shell transition metal complexes. DMRG

was first used in physics to describe spin-spin correlations in a more refined way than can be achieved with a mean-field approach [12]. The DMRG algorithm was originally devised for chain-like systems or lattices, and thus the first applications aimed at predicting magnetically coupled systems involved linear chains of open-shell metals [89–91]. However, in these studies the electronic states are not constructed as many-electron wavefunctions as is the case in quantum chemical calculations. As such, DMRG is not a fundamentally new method for describing molecules, but rather a new algorithm that is effectively used as a CI-solver.

The algorithm differs from other CI approaches in that it stores the wavefunction in a different numerical representation than that typically encountered in CASSCF calculations. The striking feature of DMRG is that in principle the full CI solution can be approximated to an accuracy typically required for chemically relevant systems with a computational cost that is normally lower scaling than other multireference methods. While the computational cost of conventional multireference approaches is exponential, and DMRG can approximate the correct solution with polynomial cost [26] for chemically relevant systems.

The DMRG algorithm benefits from proper choice of orbital shape and ordering to achieve a desired level of accuracy while minimizing the computational cost in solving the CI problem. A key aspect is that only a few orbitals are treated exactly during each substep of the iterative procedure, and the other orbitals are either part of the so-called active subsystem or the complementary subsystem. Thus, the orbitals sequentially become part of what is known as the “exactly represented subsystem,” a set of neighboring spatial orbitals. Once each orbital has been treated exactly, i.e., after a series of microiterations, a macroiteration or *sweep* is completed. The wavefunction is represented in the product space of all orbitals, restricted to the desired total number of electrons and spin state. The number of basis states in the active and complementary subsystems is denoted by M . For two spatial orbitals in the exactly represented subsystem, the number of states is 16, as both orbitals can be in any of four occupations (doubly occupied, singly occupied spin up, singly occupied spin down, and unoccupied). The algorithm involves a step known as *blocking*, where the active subsystem is enlarged by the adjacent orbital from the exactly represented system, leading to a dimension of $4M$ for the increased active subsystem. To obtain a system size of M again, the following step is to transform the system to a new many-particle basis and thus reduce its size. This step, the transformation from a $M \times 4M$ matrix to an $M \times M$ matrix, is called *renormalization* and involves the diagonalization of the reduced density matrix. The choice of which elements to discard is based on the weights of the corresponding eigenstates, and the effect is measured as the so-called *discarded weight*. With the renormalized system, the next microiteration can start, in which the active system is enlarged by one, the exactly represented system loses one old member and gains one new member, and the complementary subsystem is diminished by one. Once the algorithm has reached the final pair of orbitals in the exactly represented subsystem, one sweep is completed. Usually several sweeps in alternating directions are performed to improve the accuracy of the DMRG representation by optimizing the representation of the complementary subsystem. The number of sweeps at a given discarded weight can be adjusted. Most DMRG implementations

have specific *sweep schedules* in which the number of renormalized basis states and sweeps is adjusted until the user-defined energy thresholds are reached.

As noted above, the DMRG algorithm in quantum chemistry packages is used as a CI-solver, and thus the result of a DMRG-SCF calculation, where DMRG-CI and orbital optimization steps alternate until convergence is achieved, should in principle be identical to that of a CASSCF calculation. The key difference between a CASSCF and a DMRG calculation lies in an additional parameter that needs to be carefully monitored and adjusted by the user in any DMRG calculation: the number of renormalized block states M , closely connected to the discarded weight and thus the accuracy of the calculation. Because a DMRG calculation does not simply converge to a preset energy criterion as a DFT or CASSCF calculation normally would, the user has to run several DMRG calculations with increasing values of M until the energy has converged to the required accuracy. The ideal value of M depends on the nature of the chemical species under investigation, on the size and character of the active space, as well as on the number of roots requested, their spin states and the type of state averaging required.

Depending on the chemical property that is targeted and the nature of the computed energies, one may be able to apply extrapolation techniques, where the full CI energy is linearly extrapolated from several calculations with increasing M [25]. It has to be noted that extrapolation from DMRG wavefunctions obtained at small M can be problematic due to the “noise” introduced deliberately in the algorithm’s initial phases [25]. The applicability of extrapolation techniques for magnetically coupled systems will be discussed in more detail in the context of the case studies presented in this chapter.

The choice of orbitals to be included in the active space, the origin of these orbitals, the localization or not, and their initial ordering are crucial decisions for a DMRG-SCF calculation and influence the convergence of the DMRG algorithm [80]. For the choice of orbitals, similar arguments can be followed as in CASSCF calculations [92]. Reiher and coworkers noted that natural orbitals from a CASSCF calculation may be better suited as starting orbitals than orbitals derived from a preceding Hartree–Fock calculation [26]. More powerful approaches rely on automated selection procedures [84, 93, 94]. For example, Stein and Reiher proposed an algorithm that employs orbital entanglement or orbital entropy measures derived from a low-accuracy, large-CAS calculation and selects the most highly entangled orbitals for the active space of the production-level calculation [84]. The initial ordering of orbitals is an important technical aspect. In general, orbitals that are more entangled should be placed closely together, but unlike in chain-like systems the optimal way of doing this is not obvious for complex non-linear molecules. Current implementations of DMRG software in quantum chemistry usually optimize and update the order of orbitals through automated reordering procedures [25, 80, 95]. Similarly, localized orbitals can improve the performance of DMRG as they help to reduce the entanglement of the system, which implies that the number of renormalized basis states to reach a certain accuracy will be lower.

DMRG enables CASCI and CASSCF calculations with active spaces containing tens of orbitals; however, only a small part of dynamic electron correlation can

be recovered by extending the active space. Therefore, additional treatments must still be applied to the DMRG-SCF wavefunction, such as second-order perturbation theory [96–99]. An example of the effect of perturbative treatment of a DMRG-SCF wavefunction in the case of a magnetically coupled system will be discussed in one of the case studies below.

DMRG has already seen a number of applications in transition metal chemistry [15, 16, 19, 20, 100–107] and its ability to handle large active spaces in exchange-coupled transition metal systems has been showcased in two papers that deal with tetramanganese cluster complexes (Fig. 1). The first one studied a minimal model of the oxygen-evolving complex of Photosystem II, a tetramanganese–calcium cluster with five oxo-bridges embedded in a protein environment composed mainly of carboxylate ligands [19]. An active space of 44 electrons in 35 orbitals was constructed from all Mn $3d$ orbitals and the oxygen $2p$ orbitals of all five bridges. A single root with the experimentally known spin multiplicity was calculated with this (44, 35) active space using DMRG-SCF and its energy was converged to 0.16 kJ mol^{-1} . Furthermore, the quantum entanglement of the cluster [83] was analyzed [19]. In another example, Paul et al. [21] studied a synthetic tetramanganese–calcium complex [108] that is considered a structural mimic [109] of the oxygen-evolving complex in Photosystem II [110], albeit lacking one flexible oxo-bridge in the center of the inorganic core [111, 112]. DMRG-SCF with a (37, 32) active space containing all Mn $3d$ and O $2p$ orbitals was used to distinguish between two isomeric forms of the complex. A single root was calculated for each isomer and the energies were converged to $10^{-4} \text{ kcal mol}^{-1}$. It is also worth mentioning a DMRG-SCF study by Sharma et al. [20] of biologically ubiquitous [113] iron–sulfur systems, specifically Fe_2S_2 dimers and Fe_4S_4 clusters. DMRG allowed the use of a (32, 30) active space for the dimers, i.e., including all Fe $3d$, $4s$, $4d$ and S $3p$ orbitals, and energies of individual spin states were converged to $0.1 \text{ kcal mol}^{-1}$ (35 cm^{-1}). For the Fe_4S_4 cluster, a Fe $3d$ and S $3p$ (54, 36) active space could be used for specific roots in DMRG-CI calculations. These three studies either did not attempt or did not conclusively address the problem of magnetic coupling in the tetranuclear systems, but the impressive feat of performing multireference calculations on systems of this size nevertheless demonstrates the impressive new possibilities offered by DMRG. At the time of this writing, only two detailed studies of the performance of DMRG-SCF for the exchange coupling problem per se exist in the literature, both on exchange-coupled transition metal dimers. In the remainder of this chapter, we present and discuss the content and insights gained from these studies.

4 Case Studies: Magnetic Coupling in Dinuclear Complexes

Studies of exchange coupling in transition metal complexes using DMRG-based multireference approaches are still rare. Consequently, the optimal ways of constructing and handling the large active spaces enabled by the DMRG approach, as

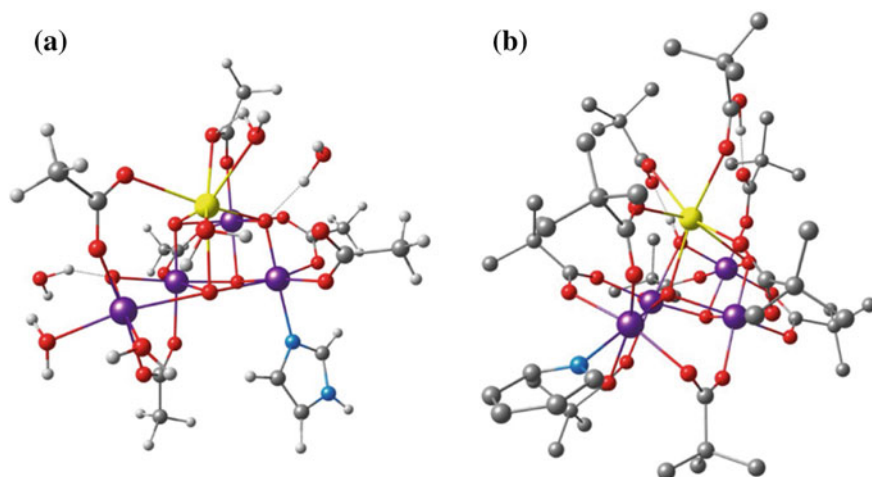


Fig. 1 Examples of oligonuclear exchange-coupled transition metal systems for which CASSCF calculations with large active spaces including all metal d and bridging ligand orbitals became tractable through the use of DMRG: **a** 79-atom simplified model of the tetranuclear $\text{Mn}_4\text{O}_5\text{Ca}$ cluster in the oxygen-evolving complex of photosystem II studied by Kurashige et al. [19] (Mn: purple; Ca: yellow; O: red; N: blue; C: gray; H: white). **b** 182-atom synthetic analogue of the OEC with a $\text{Mn}_4\text{O}_4\text{Ca}$ core [108] studied by Paul et al. [21] (right, hydrogen atoms omitted for clarity). Single-root DMRG-SCF calculations for these two systems were reported with (44, 35) and (37, 32) active spaces, respectively

well as the technical parameters that define the best usage of the method remain under investigation. In the following, we will discuss two landmark case studies on exchange-coupled dinuclear transition metal complexes that have contributed toward clarifying these points.

4.1 *Fe₂ and Cr₂ Mono- μ -Oxo Complexes*

For two mono- μ -oxo-bridged dinuclear complexes exhibiting antiferromagnetic coupling, $[\text{Fe}_2\text{OCl}_6]^{2-}$ and $[\text{Cr}_2\text{O}(\text{NH}_3)_{10}]^{4+}$ (Fig. 2), Harris et al. studied the effects of basis set choice, number of renormalized basis states M , and active space composition on the predicted exchange coupling constant J [22].

In the iron complex, the single oxo-bridge can engage in σ - and π -bonding with the Fe(III) ions. The authors chose a considerably bent geometry in which the Fe- μ -O bond lengths are 1.761 Å, and the Fe-O-Fe angle is 144.6°. It should be noted that this might have not been an optimal choice of either reference system or geometry because an earlier paper by Lledós et al. had shown that the bent form is the result of weak intermolecular interactions in the crystal, suggesting that only linear Fe-O-Fe conformations are found in solution [114]. Experimentally, the magnetic susceptibil-

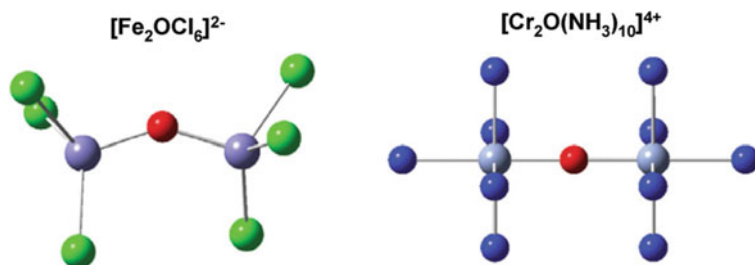


Fig. 2 Two mono- μ -oxo-bridged complexes studied by Harris et al. The hydrogen atoms of the NH_3 ligands have been omitted for clarity. Reprinted from [22] with the permission of AIP publishing

ity was very difficult to fit due to the simultaneous presence of linear and bent forms in the powdered sample. Based on B3LYP or B3LYP-derived absolute magnitudes and relative differences between the linear and bent forms, Lledós et al. suggested fitted exchange coupling constants of -117 or -119 cm^{-1} for the bent and -133 or -130 cm^{-1} for the linear form. The magnetic coupling constants computed with B3LYP were in fact significantly smaller ($J_{\text{lin}} = -84 \text{ cm}^{-1}$, $J_{\text{bent}} = -73 \text{ cm}^{-1}$) than the B3LYP ones ($J_{\text{lin}} = -145 \text{ cm}^{-1}$, $J_{\text{bent}} = -161 \text{ cm}^{-1}$) [114]. The coupling strength used as the “experimental” reference value by Harris et al. was -117 cm^{-1} [22].

The Fe(III) ions have locally high-spin d^5 configurations. The Heisenberg spin ladder produced by the coupling of the two local $S_A = S_B = 5/2$ spins thus consists of the six spin states $S = 0, 1, 2, 3, 4,$ and 5 . The minimal active space is composed of 10 electrons in 10 d orbitals, (10, 10). Including the occupied μ -O bridge O($2p$), orbitals result in a (16, 13) full-valence active space. Both of these spaces can be treated at the CASSCF level. Assuming a regular Landé spacing, that is, an energy difference of $2J$ between the $S = 0$ and the $S = 1$ states, the predicted magnetic coupling constant was -39.7 cm^{-1} for the minimal active space and -58.6 cm^{-1} for the full-valence active space. Both fall short of the reference value of -117 cm^{-1} . Without further active space expansion, the experimental value can be approached using the (16, 13) active space with multireference configuration interaction calculations including the Davidson correction (MRCI+Q), which yields a value of -115.3 cm^{-1} for the exchange coupling constant.

Expansion of the active space with unoccupied metal and ligand orbitals leads to active space sizes that can only be described with the DMRG approach. Upon inclusion of the ten $4d$ orbitals to the metal-only (10, 10) active space, leading to a CAS(10, 20), the antiferromagnetic exchange coupling is strengthened to -49.0 cm^{-1} . Inclusion of only the μ -O $3p$ orbitals on top of the full-valence active space, i.e., (16, 16), leads to a coupling constant of -57.7 cm^{-1} and is hence insufficient for a quantitative agreement with experiment. However, inclusion of both metal and bridge virtual orbitals to the full-valence active space, resulting in a (16, 26) active space, was shown to yield a projected magnetic coupling constant of -117.4 cm^{-1} , in quantitative agreement with the experimental value.

The above observations can be rationalized in terms of charge-transfer configurations when virtual orbitals are included in the active space. By adding bridge $3p$ orbitals, metal-to-ligand charge transfer (MLCT) configurations are considered. Analogously, the inclusion of a metal “double shells” adds ligand-to-metal charge transfer (LMCT) configurations and introduces radial dynamic correlation. In a traditional CASSCF calculation, the individual configurations and their relative contributions can be analyzed and quantified in a relatively straightforward manner; however, the weights of contributing configurations [88, 115] were not reported from the DMRG calculations. Nevertheless, as an indirect or summative effect of all CT configurations, the orbital contour plots revealed the contribution of LMCT states as a more pronounced delocalization on the bridging ligands.

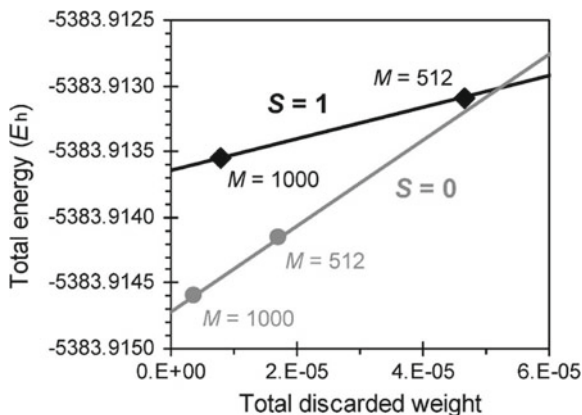
The effect of basis set choice on the exchange coupling constant was studied in some detail. The calculations employed relativistic atomic natural orbital basis sets (ANO-RCC) with a series of contractions. For both the CASSCF(16, 13) and DMRG-SCF(16, 26) calculations, a larger basis set led to weaker exchange coupling. For the CASSCF approach, the results were converged with a quintuple- ζ basis set for iron and oxo-bridge, and a quadruple- ζ basis set for the peripheral chloride ligands. For the DMRG approach, the convergence behavior is less clear, as there is an additional strong dependency on the M value: larger basis sets require a larger M , but as this creates higher memory demands the calculations are not always feasible. The basis set convergence is very similar for the CASSCF and DMRG approaches as long as M is sufficiently large, i.e., up to a quadruple- ζ basis for all elements. It should be noted that although no chloride orbitals enter the active space, increasing the basis set size from double- ζ to quadruple- ζ was reported to change the predicted exchange coupling constants by ca. 5 cm^{-1} . This may be related to the π -bonding between chloride and the iron ions. Taking both accuracy and efficiency into account, Harris et al. [22] opted for a triple- ζ basis set for iron and oxygen, and a double- ζ basis set for the peripheral chloride ligands.

The number of renormalized basis states, M , must be sufficiently large to ensure that the energy converges to the correct value for a given choice of active space. Furthermore, larger active spaces require larger values of M to converge properly, implying that across a series of calculations with varying active space sizes for the same system, different numbers of renormalized basis states will be needed. Because the energy of a system converges to the exact value for increasing values of M , i.e., decreasing discarded weights, a linear extrapolation can be used to find the exact energy based on several calculations with different numbers of renormalized basis states.

The convergence with M is different for different spin states. This is apparent, for example, in the case of the iron dimer (Fig. 3) [22]. The extrapolation of the $S = 0$ state has a steeper slope than the extrapolation of the $S = 1$ state, both based on two energies calculated with $M = 512$ and $M = 1000$. It is also noted that the corresponding discarded weights differ for calculations of different spin states with the same M value.

When aiming to predict accurate energies of different spin states of an exchange-coupled system to subsequently extract coupling constants measured in cm^{-1} units

Fig. 3 Extrapolation of DMRG(12, 26) energies to infinite M for the singlet and triplet states of $[\text{Fe}_2\text{OCl}_6]^{2-}$. Reprinted from [22] with the permission of AIP publishing



of energy, one needs to take into account that a 1 cm^{-1} energy difference corresponds to $4.556 \times 10^{-6} \text{ Eh}$. The question of which M is sufficient in the case of the μ -oxo-bridged dimer was studied by comparing the CASSCF(16, 13) energies with the DMRG-SCF energies calculated with $M = 64, 128, 256$. A micro-Hartree energy difference is achieved between $M = 128$ and $M = 256$, and the latter energy is within $0.2 \mu\text{Eh}$ of the CASSCF energy. Of course, the CASSCF energy difference itself is insufficient to extract quantitatively correct exchange coupling constants, but it can serve as a valid reference point. For larger active spaces without CASSCF reference energies, Harris et al. increased M until the change in energy was less than $1 \mu\text{Eh}$, resulting in $M = 1000$ for (16, 16), whereas for the (10, 20) active space $M = 256$ was considered sufficient [22]. For the (16, 26) active space, the energy change for $M = 512$ and $M = 1000$ was ca. $500 \mu\text{Eh}$, but the authors opted to extrapolate these two values to deduce the exchange coupling constant. This resulted in the value that gives the best agreement with the experimental reference of -117 cm^{-1} .

Given that different spin states converge differently with respect to M , it seems strongly advisable to test the convergence behavior of all spin states of a magnetically coupled system instead of only two. As will be discussed in greater detail for the second case study on a manganese dimer, low M values can lead to non-Landé spin-state patterns, meaning that without having calculated the full spin ladder, it cannot be known whether the $S = 0$ and $S = 1$ states are actually correctly computed with respect to the other states, or indeed if they actually are the lowest energy states predicted by the method for the given choice of active space and M .

The second example in the study of Harris et al. was the antiferromagnetically coupled chromium dimer $[\text{Cr}_2\text{O}(\text{NH}_3)_{10}]^{4+}$, with a linear Cr–O–Cr angle and Cr–O bond lengths of 1.821 \AA [22]. The ammonia ligands were placed at unoptimized average crystallographic distances of 2.12 \AA from the chromium ions, and the hydrogen atoms were optimized. The chromium ions are in their +III oxidation states, with a d^3 electronic configuration ($S_A = S_B = 3/2$), leading to a spectrum of four coupled

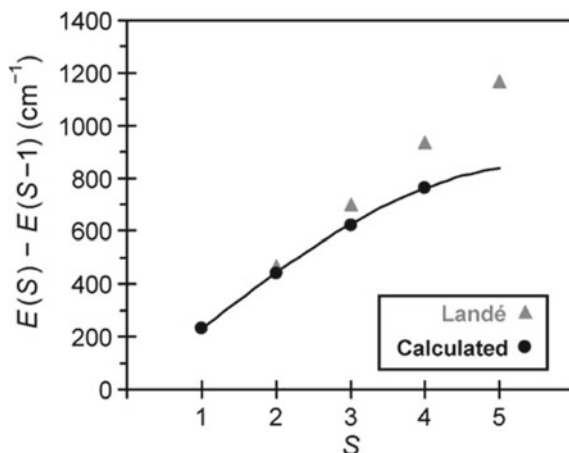
spin states, $S = 0, 1, 2,$ and 3 . The experimentally determined exchange coupling constant is -225 cm^{-1} .

Similar to the iron dimer, a triple- ζ basis set for chromium and oxygen, and a double- ζ basis set for the peripheral ammonia ligands was chosen. The minimal active space is a (6, 6) active space containing only the magnetic orbitals. CASSCF with this active space produces an exchange coupling constant of -52.4 cm^{-1} . The expansion of the active space to include occupied bridge orbitals as well as virtual orbitals was described in this study as much more challenging. Upon inclusion of the occupied $2p$ as well as the virtual $3p$ oxo-bridge orbitals, the exchange coupling strength increases to -60 cm^{-1} with CASSCF. The authors attempted to include the empty Cr d orbitals in the active space, but only a (12, 13) CAS could be converged, which contained an orbital delocalized over the entire core. It had $d(z^2)$ character on both metal centers, and symmetrical nodal planes with a lobe of s -character on the oxo-bridge. Although still not containing all metal d orbitals, the exchange coupling constant increases to -92.8 cm^{-1} . The authors attributed this improvement to a more balanced description of the Cr–O σ bonds, achieved by symmetrical mixing of the orbitals dominated by O $p(z)$ and Cr $d(z^2)$ character. From a pure MO theory point of view, one would expect three orbitals in total to be of importance for the σ bonds: one dominated by the O $p(z)$ atomic orbital (no nodal plane), and two dominated by Cr $d(z^2)$ character (one and two nodal planes).

Using an active space of (12, 25), containing the magnetic orbitals and their double shells as well as the oxo-bridge $2p$, $3p$, and $3d$ orbitals, a stronger antiferromagnetic coupling can be achieved. With $M = 512$ the exchange coupling constant J is -166.9 cm^{-1} , but increasing M to 1000 results in an exchange coupling constant that is significantly weaker, $J = -137.9 \text{ cm}^{-1}$. Extrapolation of the individual state energies to zero discarded weight results in an exchange coupling constant of -123.6 cm^{-1} , ca. 100 cm^{-1} lower than the experimental value. In terms of possible charge-transfer excitations with this active space, the MLCT excitations would be expected to be adequately represented given that all magnetic orbitals and relevant virtual ligand orbitals are included in the active space. In contrast, LMCT excitations must be more limited, given that the virtual chromium $3d$ orbitals and their double shells are not taken into account, and therefore dynamic correlation is recovered incompletely compared to other systems.

An active space that contains a larger number of chromium $3d$ and $4d$ orbitals is the (12, 32) active space. All $3d$ orbitals, the $4d(xy)$, $4d(xz)$, $4d(yz)$, and one $4d(z^2)$ orbital are included. Additionally, the $2p$, $3s$, $3p$, $3d$, and $4p$ orbitals of the central oxo-bridge are taken into account. With this active space, an exchange coupling constant of -165.9 cm^{-1} is achieved, with $M = 1000$ and a very small basis set (Cr: double- ζ , O: triple- ζ , N, H: single- ζ). Extrapolation was not possible in this case due to convergence problems of the $M = 512$ calculation. It was also shown that the basis set effect in this system is considerable. For the (12, 25) active space, a 11.8 cm^{-1} difference results between the double- ζ and triple- ζ basis sets on Cr and O. With a larger basis set, it might be hoped that an improved exchange coupling constant could be achieved; however, the available results strongly indicate that this active

Fig. 4 Deviation from the Landé interval rule for the $[\text{Fe}_2\text{OCl}_6]^{2-}$ complex, calculated with DMRG(16, 26) and $M = 1000$. The computed data are fit with a biquadratic term in the Hamiltonian. Reprinted from [22] with the permission of AIP publishing



space is inadequate to approximate the experimental value of -225 cm^{-1} , regardless of basis set size and M convergence.

In all of the above results and the related discussion, the exchange coupling constant was calculated exclusively from the energy difference of the $S = 0$ and $S = 1$ states. As described in the introduction, deviations from the Landé interval rule can be indicators of biquadratic exchange [116, 117]. For the iron dimer, Harris et al. reported significant deviations from the expected splitting, whereby for the CASSCF(10, 10) calculations the exchange coupling constant calculated from the $S = 1$ and $S = 0$ energy difference is -41.2 cm^{-1} , whereas from the $S = 4$ and $S = 5$ energy difference J is calculated as -27.9 cm^{-1} . Similarly, for the largest active space treated at DMRG level, (16, 26), the range of magnetic coupling constants predicted for different adjacent energy levels ranges from -95.4 to -116.8 cm^{-1} , although the real span might be slightly larger considering that, curiously, the calculation for the ferromagnetic (and hence single determinantal) $S = 5$ state could not be completed in this study (Fig. 4). The deviation was fit with a biquadratic term; however, no experimental data are available to verify whether this is necessary or physically valid. For the chromium dimer, similar trends are found: the exchange coupling constants for the smallest active space range from -45.5 to -52.4 cm^{-1} depending on the spin-state interval they are derived from, and for the DMRG-SCF(12, 25) active space the magnetic coupling constants range between -115.4 and -137.9 cm^{-1} .

Importantly, this latter finding is at odds with a subsequent paper by Spivak et al. [118], who studied precisely the same system with an approach that combined state-averaged CASSCF orbitals with partially contracted N -electron valence second-order perturbation theory (NEVPT2) calculations. In the study by Spivak et al. [118], it was reported that the exchange coupling constants derived from the different pairs of spin states (singlet–triplet, triplet–quintet, and quintet–septet) are all very similar and that no significant deviations from the Landé pattern were observed, in stark contrast to the DMRG results of Harris et al. The crucial difference between the two

studies appears to be the method of orbital optimization: Harris et al. reported results from state-specific calculations, whereas Spivak et al. used state-averaged orbitals, i.e., a common set of orbitals for all spin states arising from the magnetic coupling of the two ions. Among other methodological points, the study of the Mn dimer by Roemelt et al. [23] to be discussed in the following investigated this issue explicitly, strongly suggesting that the use of state-averaged orbital optimization is necessary to avoid spurious and often unphysical deviations from the regular spacing of magnetic levels.

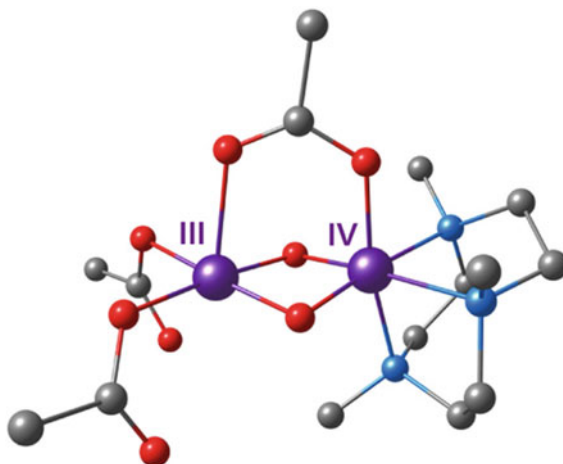
4.2 *Mn₂ Bis- μ -Oxo/ μ -Acetato Complex*

Another example of a detailed investigation of DMRG-based approaches comes from Roemelt et al. [23], who presented an in-depth study of a mixed-valence bis- μ -oxo/ μ -acetato-bridged Mn(III/IV) dimer (Fig. 5). This complex was synthesized and characterized by Bossek et al. [119], and features one 1, 4, 7-trimethyl-1, 4, 7-triazacyclononane, and two additional acetates as terminal ligands. Owing to the combination of mixed-valence and asymmetric ligation, the Mn ions adopt distinct coordination environments. The Mn(III) site features a strong axial pseudo-Jahn–Teller elongation, a hallmark of occupation of the σ -antibonding orbital of $d(z^2)$ parentage, that leads to an approximately square–pyramidal coordination geometry. This type of system is of particular interest in inorganic and bioinorganic chemistry because the high-valent nature of the Mn ions, the chemical nature of the ligands and the bridging topology are of direct relevance to manganese systems encountered widely in molecular magnetism and bioinorganic catalysis [108, 120, 121]. A prominent example in the latter case is the oxo/carboxylato-bridged Mn_4CaO_5 cluster of the oxygen-evolving complex of photosystem II, the site of water oxidation in biological photosynthesis [112, 122].

The two ions have local high-spin configurations, d^4 for Mn(III) and d^3 for Mn(IV), with corresponding local spins $S_A = 2$ and $S_B = 3/2$. These couple to produce a ladder of four spin states with total spin $S = 7/2, 5/2, 3/2$, and $1/2$. The complex exhibits antiferromagnetic coupling, therefore the spin doublet is the ground state. Magnetic susceptibility measurements led to a fitted value for the exchange coupling constant of $J = -90.0 \text{ cm}^{-1}$. Assuming the ideal case of an isotropic bilinear term in the Heisenberg Hamiltonian, the energy splittings for the spin states correspond to the Landé pattern, i.e., the $S = 3/2$ state is $3J$ higher than the $S = 1/2$ ground state, the $S = 5/2$ state is $5J$ higher than the $S = 3/2$ state, and the ferromagnetic $S = 7/2$ state is $7J$ higher than the $S = 5/2$ state, yielding a total span of $15J$ for the spin ladder.

The minimal active orbital space consists of the metal $3d$ orbitals, i.e., an active space of 7 electrons in 10 orbitals, (7, 10). Regardless of the origin of the starting orbitals or of the method used in producing localized input orbitals (e.g., Pipek–Mezey or Foster–Boys), a simple CASCI treatment was reported to lead always to strong ferromagnetic coupling ($S = 7/2$ ground state) with an exchange coupling constant J of almost $+180 \text{ cm}^{-1}$, in profound qualitative disagreement

Fig. 5 Structure of the bis- μ -oxo/ μ -acetato-bridged manganese dimer studied by Roemelt et al. Hydrogen atoms are omitted for clarity. Reprinted with permission from [23]. Copyright 2018 American chemical society



with experiment. This indicates that orbital optimization is essential for a physically meaningful treatment of the problem. CASSCF(7, 10) calculations indeed change the picture drastically, leading to an $S = 1/2$ ground state. However, at this point a very important observation was made with respect to the method of orbital optimization.

Specifically, when the orbitals of each spin state were optimized individually (state-specific orbital optimization), the relative energies of the four spin states did not follow a regular pattern: the $S = 1/2$ ground state was followed by the ferromagnetic $S = 7/2$ at 12 cm^{-1} , then the $S = 3/2$ state at 16 cm^{-1} and finally the $S = 5/2$ at 28 cm^{-1} . This order of states was confirmed to be the converged result of state-specific CASSCF(7, 10) calculations irrespective of various technical and methodological details. Hence, even though the spin-doublet state turns out to be the lowest in energy, the description of the electronic structure is fundamentally deficient and the results are of no use in the discussion of magnetic properties.

The alternative to state-specific orbital optimization is the state-averaged approach, where a common set of orbitals is obtained as the result of the CASSCF procedure, assigning equal weights to the four states that are optimized simultaneously. Note that this state-averaged approach does not refer to averaging over multiple roots of the same spin multiplicity, but averaging over the lowest root of all the different spin multiplicities that are relevant to the spin-coupling problem, in the present case the lowest root of the $S = 1/2$, $S = 3/2$, $S = 5/2$, and $S = 7/2$ states simultaneously. These state-averaged CASSCF(7, 10) calculations correctly predict antiferromagnetic coupling with a regular Landé progression and spacing of spin states. However, the computed antiferromagnetic coupling at this level was extremely weak ($J = -1.6 \text{ cm}^{-1}$) and hence the spin ladder was predicted to be highly compressed, spanning merely 24 cm^{-1} .

In comparison to the state-specific CASSCF(7, 10) results, the qualitative success of the state-averaged CASSCF(7, 10) calculations was directly attributable to the use of a common set of orbitals for all states. On the other hand, the quantitative failure

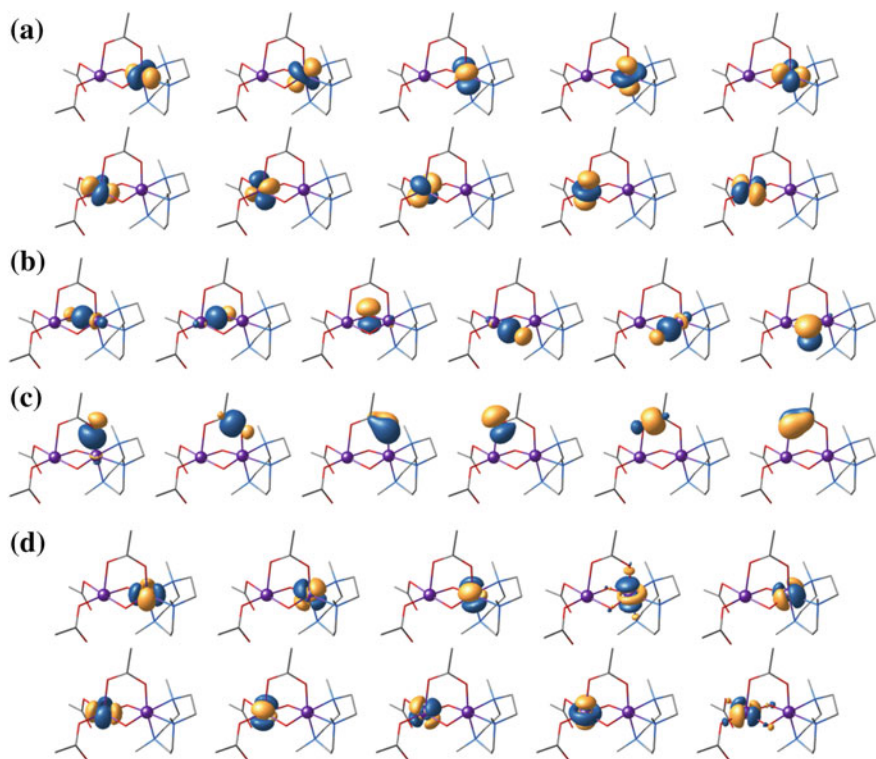


Fig. 6 Localized orbitals employed in the construction of the various active spaces described in the study of Roemelt et al. **a** Mn $3d$ orbitals; **b** O $2p$ orbitals; **c** OAc $2p$ orbitals; and **d** Mn $4d$ orbitals. Reprinted with permission from [23]. Copyright 2018 American chemical society

to approximate the experimental magnitude of the antiferromagnetic coupling was attributed to the exclusion of bridging orbitals from the active space. Subsequent calculations extended the active space to include orbitals of the oxo-bridges, of the acetato bridge, as well as “double-shell” $4d$ orbitals of the Mn ions and $3p$ orbitals of the oxo-bridges (Fig. 6), relying on DMRG to enable multireference calculations with exceedingly large active spaces.

Inclusion of the valence $2p$ orbitals of the oxo-bridges leads to a (19, 16) active space. DMRG-CI calculations without reoptimizing the CASSCF (7, 10) metal-based orbitals or the newly introduced localized orbitals of the oxo-bridges led to a considerable increase in the magnitude of the antiferromagnetic coupling, from less than -2 to -29 cm^{-1} . Subsequent orbital optimization with state-averaged DMRG-SCF calculations at increasing M values (see below) eventually yielded a converged value for J of almost -59 cm^{-1} , i.e., approximately two-thirds of the experimental exchange coupling constant. Extension of the active space by inclusion of acetato orbitals, leading to a (31, 22) active space, did not afford any further improvement. In terms of physical insight into the specific system, the above results

demonstrate that antiferromagnetic interaction in the Mn dimer arises exclusively through superexchange via the oxo-bridges and that the acetato ligand plays no role in mediating the spin coupling.

A crucial methodological point that was encountered again, even with the more extended active spaces, concerns the use of state-specific versus state-averaged orbital optimization procedures. In contrast to the state-specific calculations with the metal-only (7, 10) active space, which did not produce a qualitatively correct order of states, spate-specific DMRG-SCF(19, 16) calculations correctly produce the ordering of spin states from $S = 1/2$ as the lowest to $S = 7/2$ as the highest. Nevertheless, the spin-state energy spacings deviate strongly from the Landé pattern that is approximated very closely by state-averaged calculations. State-specific calculations produce a strong compression of the spin ladder at progressively higher spin levels, which is particularly exaggerated at low values of M . A crucial observation was that even with fully individually converged absolute energy values (at $M = 2000$) state-specific calculations underestimate the stability of the intermediate $S = 3/2$ and $S = 5/2$ states and overestimate the stability of the high-spin $S = 7/2$ state. The result is that at the level of accuracy required for description of magnetic levels, no meaningful exchange coupling constant can be extracted because the J values computed from energy differences between adjacent levels range from -75 cm^{-1} for the energy difference between the two lowest spin states to -44 cm^{-1} for the energy difference between the two highest spin states.

Importantly, by simply using the energy difference between the two lowest states from state-specific calculations, a deceptively “good” value for J would result, and this effect would be exaggerated at low M values (<1000). These results clearly demonstrate that the method of orbital optimization and the careful examination of convergence with M for all states of the spin ladder are essential for successful applications of DMRG-based approaches to exchange coupling problems.

A second methodological point concerns the convergence with M of the exchange coupling values obtained by state-averaged DMRG-SCF(19, 16) calculations. Table 1 reproduces some of the results from the Roemelt et al. study [23], showing the evolution of the energy levels with the number of renormalized states. The smallest value reported was $M = 250$ because smaller values either led to numerically scattered results or failed to converge. The $M = 250$ results are not physically meaningful as they show no reasonable relation between the spin levels, strongly underestimating the stability of the intermediate $S = 3/2$ and $S = 5/2$ states. $M = 500$ is an improvement but must be considered similarly unusable because of the large differences of the J value obtained for different pairs of states. For $M \geq 1000$, the average J value is converged, but further small improvements are observed up to the highest tested $M = 3000$ with respect to the energy of individual spin states, particularly the $S = 3/2$ state.

In an attempt to further improve the numerical result for the exchange coupling constant, virtual orbitals of the Mn ions (the “double shell” of $4d$ orbitals) were included in the active space. DMRG-CI(19, 26) calculations demonstrated a small increase in the antiferromagnetic interaction ($J = -65 \text{ cm}^{-1}$). This improvement was however negated by the further expansion of the active space to include the $3p$

Table 1 Energy differences (cm^{-1}) between spin states of the mixed-valence Mn dimer reported by Roemelt et al. [23]. The results are from state-averaged DMRG-SCF calculations with a (19, 16) active space composed of Mn $3d$ and O $2p$ orbitals for different numbers of renormalized states M . Pairwise exchange coupling constants and the average J value (cm^{-1}) are reported for each M . Adapted with permission from [23]. Copyright 2018 American chemical society

S	$M = 250$	$M = 500$	$M = 1000$	$M = 2000$	$M = 3000$
$7/2$	775.3	868.2	878.7	879.9	879.9
$5/2$	694.8	486.3	476.3	475.9	475.9
$3/2$	490.1	215.0	182.6	180.6	180.4
$1/2$	0.0	0.0	0.0	0.0	0.0
$J_{(7/2-5/2)}$	-11.5	-54.6	-57.5	-57.7	-57.7
$J_{(5/2-3/2)}$	-40.9	-54.3	-58.7	-59.1	-59.1
$J_{(3/2-1/2)}$	-163.4	-71.7	-60.9	-60.2	-60.1
J	-71.9	-60.2	-59.0	-59.0	-59.0

orbitals of the oxo-bridges, as DMRG-CI(19, 32) calculations yielded a value of $J = -60 \text{ cm}^{-1}$. These results suggest that at the CASCI level the virtual orbitals play a secondary role and their inclusion is not sufficient to overcome the principle limitations of the approach, namely the incomplete account of dynamic correlation.

Full state-averaged orbital optimization could not be completed with the (19, 32) active space; however, DMRG-SCF calculations could be successfully driven to completion with the (19, 26) active space. The latter were reported to be extremely challenging in terms of convergence, but even when converged, the results revealed a new complication. This was the highly increased sensitivity to the M value that resulted in strong deviations from the normal inter-level energy spacing even at the highest applicable $M = 1500$. Clearly, what constitutes a sufficient value for M is entirely dependent on the nature and composition of the active space. As an example, although $M = 1000$ was perfectly adequate in DMRG-SCF calculations with the (19, 16) active space, when the $4d$ metal orbitals were included in the active space the pairwise values for the exchange coupling constants at $M = 1000$ were $J_{(7/2-5/2)} = -39 \text{ cm}^{-1}$, $J_{(5/2-3/2)} = -73 \text{ cm}^{-1}$, and $J_{(3/2-1/2)} = -142 \text{ cm}^{-1}$, precluding any interpretation. At $M = 1500$, these values improved to $J_{(7/2-5/2)} = -61 \text{ cm}^{-1}$, $J_{(5/2-3/2)} = -75 \text{ cm}^{-1}$, and $J_{(3/2-1/2)} = -97 \text{ cm}^{-1}$, which is still far from convergence. Thus, it was concluded that values of M significantly higher than what was technically possible at that point would be necessary to produce converged results. On the other hand, it was noticed that the incoherent results were mostly due to the relative energies of the two intermediate spin states and that the total span of the ladder, i.e., the energy difference between $S = 1/2$ and $S = 7/2$, was less sensitive to the increasing M . This observation allowed the estimation that the full effect of the Mn $4d$ orbitals would be a ca. 10 cm^{-1} enhancement of the antiferromagnetic coupling.

The study of the manganese dimer concluded that the enormously increased cost and effort of obtaining reasonably converged state-averaged DMRG-SCF results for active spaces considerably larger than the full-valence (19, 16) space of Mn $3d$ and O $2p$ orbitals, particularly for active spaces that include virtual orbitals, is neither justified by the limited numerical improvements nor expected to eventually produce quantitatively satisfying results. Instead it was suggested that similarly to the standard use of dynamic correlation methods such as CASPT2 and NEVPT2 on top of a CASSCF reference, the full-valence DMRG-SCF wavefunction could be used in subsequent DMRG-NEVPT2 calculations.

Indeed, DMRG-NEVPT2 calculations with the (19, 16) active space produced an average J value of -85 cm^{-1} (converged at $M' = 1500$), in very good agreement with the experimental value. Compared to the DMRG-SCF calculations with the same active space, a larger number of retained states were required for satisfactory convergence of the NEVPT2 calculations, because of the requirement to calculate reduced density matrices for more than two active electrons. Importantly, the variations of J values obtained from different spin-state pairs by DMRG-NEVPT2 was less than 1 cm^{-1} , confirming the prediction of Heisenberg behavior by the state-averaged DMRG-SCF calculations.

5 General Remarks

5.1 Active Space Composition

A common choice in the case studies mentioned above is that the smallest useful active space in practice contains the metal d orbitals as well as the valence orbitals of the bridging ligands. Although the results obtained from DMRG-SCF calculations with a metal-only active space are typically not numerically or qualitatively useful in themselves, this does not mean that an active space composed of only metal-based orbitals is a meaningless choice in principle. In certain types of application, this can indeed form a well-defined starting point for certain computational approaches, such as the difference-dedicated configuration interaction approach (DDCI) that attempts to introduce a posteriori all the important corrections which are by definition absent from the small reference wavefunction. However, these approaches lack generality because of their extremely restricted field of application given their enormous cost. The point of using DMRG is precisely that the severe restrictions on the size of the active space can be lifted at the reference level, which not simply extends the applicability of multireference methods to any exchange-coupled transition metal system but, importantly, allows explicit inclusion of a large part of the required physics directly into the reference wavefunction. Therefore, we consider the inclusion of all metal and ligand valence orbitals to be the natural minimal choice in DMRG-based studies of exchange-coupled systems.

On the other hand, the question of whether virtual orbitals of the metal ions and the bridging ligands are required in the active space, for example, the double shell of $4d$ orbitals in the case of $3d$ metal ions, does not appear to have a straightforward and universal answer based on the existing studies. It is clear that these orbitals have an effect, which can be attributed in part to further recovery of dynamic correlation or incorporation of specific excitation classes, but the magnitude of this effect appears to be system-dependent. Therefore, this type of active space extension should be evaluated in combination with the estimated gains and in relation to the relative cost. This point became obvious with the MRCI+Q results in the study of Harris et al. [22] and was further discussed in the study of Roemelt et al. where it was judged that the steep increase in cost outweighs the gains, particularly if one considers that the “missing” part of the exchange coupling interaction is unlikely to be sufficiently recovered by the double-shell extension of the active space and can be more conveniently accounted for with the DMRG-NEVPT2 approach [97].

However, this is likely not a general result. The conclusion may be in part due to the fact that the d shell of the Mn ions is less than half-filled. In cases where the double-shell effect is strong, it is expected that it has to be treated as part of the static correlation [123] and included directly in the orbital optimization. In addition, CASPT2/NEVPT2 energies in general react more sensitively to the double-shell effect than CASSCF. Although no general guideline with respect to the treatment of virtual orbitals can be given at this stage, we expect that the increasing use of automated or semi-automated active space selection procedures based on entanglement measures [84] will enable a more efficient and systematic approach to determining active space composition for DMRG-SCF calculations on exchange-coupled systems.

5.2 *Orbital Optimization, State Selection and Convergence*

Besides the definition of the active space, a decision that crucially determines the nature of results and conclusions concerns the states targeted and the method employed for orbital optimization, given that the form of the active orbitals has a crucial effect on the prediction of magnetic properties [124]. Of the case studies discussed above, only the work of Roemelt et al. [23] contrasted explicitly the results of state-specific versus state-averaged orbital optimization. The study of the Mn dimer vividly demonstrated that state-specific CASSCF calculations with a metal-only active space lead to erratic results, while state-specific DMRG-SCF calculations with a full-valence active space, even though not producing qualitatively unreasonable values, still lead to large and experimentally incompatible deviations from the Landé spacing of spin states. It was concluded that state-averaging is the preferred approach because it minimizes these artificial deviations from the Landé pattern. This means that the orbital optimization procedure should produce simultaneously orbitals equally good for *all* states of the spin ladder that describe the magnetic interaction in the exchange-coupled system.

As a corollary, extraction of a hypothetical exchange coupling constant J based on only two computed states using state-specific calculations is unreliable because the assumption of a Landé pattern may not hold at all. With the energies of only two states, whether they are assumed to be the two lowest energy ones or the states with highest and lowest spin multiplicity for a given spin-coupling situation, one could still remain blind to potentially fundamental deficiencies in the description of the electronic structure of the system. State-averaged orbital optimization can obviously be more expensive than a state-specific approach, but as a counterweight it usually has the advantage of more efficient convergence of the CASSCF procedure, associated with the treatment of all states arising from a given electronic configuration. In this respect, it should be realized that both the inability to adequately approximate an experimental exchange coupling constant and the encounter of convergence problems for specific magnetic states may not be due to active space selection but due to the choice of the orbital optimization procedure. This may relate, for example, to the observation of Harris et al. that certain spin states of the chromium dimer could not be converged (in state-specific calculations) for specific choices of M and active space [22].

State-averaged orbital optimization does not automatically eliminate Landé deviations; there is still a strong dependence of the relative energies of the spin states on the number of retained states M , as shown in Table 1. Therefore, state-averaged orbital optimization should be combined with careful examination of the convergence with M of pairwise energy differences between the different spin states in order to determine the point where converged values for the exchange coupling problem can be obtained. It is important to note that at small values of M , the results on the Mn dimer can be considered numerically unstable [23], but results obtained with such small M values have been used in extrapolating spin-state energies in the study of Harris et al. [22]. It will be interesting to see the effect of state-averaged orbital optimization in the case of the Fe and Cr dimers. It is clear in both studies that regardless of the method employed for orbital optimization, different spin states converge at different rates with increasing M . The energies of individually optimized spin states can in principle be extrapolated to infinite M (see Fig. 3), whereas it is not clear how this can be performed in the case of state-averaged results, especially when the discarded weight for all states becomes negligible at high enough M values [23]. Further studies of exchange-coupled systems will be required to better evaluate the various methodological parameters relating to spin state selection, orbital optimization, and convergence of relative energetics with M . An important question to clarify for large-active-space DMRG-SCF calculations is whether it will be possible to avoid or relax the requirement for state-averaged orbital optimization over the complete span of the spin ladder, because this seriously limits the nuclearity of the complexes that can be successfully treated.

5.3 Deviations from Heisenberg Behavior

From the preceding discussion, it can be concluded that if a state-averaged approach is required for the qualitatively correct description of magnetic levels, then the use of state-specific DMRG-SCF calculations to predict *deviations* from Heisenberg behavior is unjustified. Such deviations can of course be perfectly physical: the isotropic bilinear Heisenberg Hamiltonian is but an idealized approximation and further terms can be invoked to account for specific observed deviations in the magnetic behavior of a system, e.g., non-Hund states [2, 125]. As such, the reproduction of a Landé pattern should not be considered as a desirable “target” for quantum chemical treatments of exchange-coupled dimers. On the other hand, the analysis of Landé deviations for the systems discussed above suggests that such deviations result from specific methodological choices, and at least in certain cases they can be viewed as artifacts of either a small active space, state-specific orbital optimization, small M , or a combination of the above, with state-averaged orbital optimization being the most important factor in avoiding such artifacts.

The computed energetics in the study of Fe and Cr dimers suggested a progressive compression of the spin ladder at higher S states (see Fig. 4) [22], which Harris et al. considered to be a genuine and physically meaningful demonstration of non-Heisenberg behavior. Consequently, they fitted the computed energies with an additional biquadratic term in the Hamiltonian. However, de Graaf and coworkers did not observe this type of deviation when they revisited one of the dimers of the Harris et al. study [118]. The critical difference in this subsequent study was the use of state-averaged orbitals, which apparently eliminated the artificial compression of the spin ladder. The direct comparison between state-specific and state-averaged orbitals by Roemelt et al. for the Mn dimer quantified explicitly the significant differences between state-specific and state-averaged results, concluding that only the latter afford a valid description of the spin ladder. One might argue that the use of state-averaged orbitals could introduce a bias toward isotropic behavior. However, this would be incorrect for two reasons: first, because the magnetic levels do normally arise from a single principle electronic configuration, and second, because the use of state-averaged orbitals does not impose an idealized isotropic spacing of the magnetic levels anyway, as demonstrated clearly from the results on the Mn dimer.

The question, therefore, is when should computed deviations be considered physically meaningful? One safe conclusion so far is that state-specific calculations are inappropriate for this problem. This has wider implications for any study that attempts to employ large-active-space DMRG calculations for the analysis of exchange-coupled systems, but even more so for studies that aspire to directly predict such deviations. An example of the latter is the investigation of double exchange in a series of iron–sulfur systems by Sharma et al. [20], who employed DMRG to study a series of iron–sulfur systems that can be considered models of the Fe/S cofactors in biological electron transfer. Among the complexes investigated was the $[\text{Fe}_2\text{S}_2(\text{SCH}_3)_4]^{2-/3-}$ pair. In the oxidized form both ions are high-spin Fe(III), with local spins $S_A = S_B = 5/2$, which lead to the same set of total spin states as for the iron dimer discussed

above, i.e. $S = 0, 1, 2, 3, 4,$ and 5 . The reduced dimer formally contains one high-spin Fe(III) ion ($S_A = 5/2$) and one Fe(II) ($S_B = 2$). This is a particularly challenging case because the additional electron can delocalize between the two iron sites. In the classic picture, this leads to the splitting of the individual Heisenberg spin levels S by a “double-exchange” term $\pm B(S + 1/2)$. Sharma et al. investigated the low-energy spectrum for this complex, albeit without performing spin-state averaging of orbitals. They noticed that the low-lying states could not be adequately described by the classical double-exchange Hamiltonian because their number was greater than what is accounted for by the classical phenomenological model as a result of multi-orbital double-exchange processes [20]. It remains to be seen how the choice of orbital optimization affects the conclusions in such electronic situations, electronically more complex than the exchange-coupled dimers discussed by Harris et al. and Roemelt et al., but potentially also more sensitive to methodological choices. At least in the more straightforward examples of the dimers discussed as case studies herein, where the spin manifold is sufficiently separated from excited electronic configurations, the quality of the results is adversely affected by the use of spin-state-specific energies.

5.4 Analysis of Exchange Coupling

The investigation by Roemelt et al. into the effect of different bridging ligands in the case of the Mn dimer by including subsets of bridge-localized orbitals in the active space established that the oxo-bridges mediate exchange coupling but that the acetato bridge plays only a structural and not a magnetic role [23, 45]. This application serves to demonstrate an important use of DMRG in exchange-coupled systems, namely that by selective inclusion of localized orbital subspaces in the multireference treatment one can systematically evaluate the contribution of distinct magnetic pathways. Thus, even if the absolute value of the computed exchange coupling constants is not in quantitative agreement with experiment, this approach enables the mapping of the “magnetic topology” of a complex. Analysis of broken-symmetry determinants along the lines of the Amos–Hall corresponding orbital transformation have long been used for qualitative analysis of superexchange pathways in DFT studies of exchange-coupled systems [33, 45], but is not directly applicable to systems with more than two spin sites [47]. By contrast, the DMRG-driven analysis based on selective active space inclusion of valence orbitals of specific groups is general and can be applied in any chemical context. Evidently, this approach is not unique to DMRG approaches. For example, Domingo et al. [126] have used standard CASPT2 calculations with localized orbitals to investigate the influence of different parts of the molecule on the overall magnetism of a series of dinuclear molecules. Still, DMRG enables this treatment to be applied to much larger systems than previously possible in terms of size, nuclearity, magnetic topology, type, and number of bridging ligands. This type of treatment should nevertheless not be viewed as “quantitative,” because of the missing contributions from dynamic correlation and possible cross-interactions.

A potentially more powerful way of analyzing exchange coupling interactions would be to use orbital entanglement measures, again in combination with localized orbital subspaces. To our knowledge, the capabilities of such an approach for investigating and defining the magnetic topology of exchange-coupled transition metal complexes are still unexplored.

6 Summary and Perspectives

The new capabilities offered by the DMRG algorithm in terms of handling large active spaces in multiconfigurational SCF calculations of exchange-coupled transition metal systems have already led to pioneering applications in dinuclear complexes. The studies discussed in this chapter demonstrate that the active space limitations of traditional CASSCF approaches can largely be lifted. This promises that a multireference description is in principle achievable for any transition metal dimer regardless of the nature and oxidation state or electron configuration of the metal ions, with active spaces that at the very least are “valence-complete” in terms of including orbitals of all bridging ligands that could mediate superexchange. However, the existing in-depth studies on dinuclear complexes also highlight a number of issues that need to be taken into account and some possible problems that need to be addressed in future applications.

First of all, it is clear that in dealing with magnetic coupling orbital optimization is essential and CI approaches do not lead to useful results. At the same time, it appears that state-averaged calculations over all different spin states of the spin ladder are required to obtain correct relative energies. This can be a major obstacle in extending DMRG-SCF to systems of higher nuclearity, not necessarily because the active space would become exceedingly large, but because state-averaged orbital optimization might not be feasible over hundreds or thousands of roots encompassing all possible spin multiplicities. On the other hand, state-specific orbital optimizations, and perhaps state-averaged but spin-specific orbital optimizations, run the risk of introducing large errors in the relative energetics that can seriously undermine the quality of the results. It is not clear at this point how this conundrum can be answered, but it will certainly be an important target of future studies. Finally, it should be recognized that DMRG-SCF calculations reported to date have not demonstrably converged in a systematically defined manner to the experimental exchange coupling constants for all dinuclear complexes investigated. It is expected that, in general, quantitative predictions will still require treatment of dynamic electron correlation to achieve high accuracy. The use of DMRG-NEVPT2 has already been demonstrated in the case of a manganese dimer but other methods need to be explored and evaluated [127–132]. DMRG-based multiconfigurational approaches offer undoubtedly a new basis not simply for obtaining numerically useful results for exchange-coupled systems but for analyzing their electronic structure, investigating their magnetic topology, and

enabling an improved understanding of their magnetic properties. The case studies discussed in this chapter simply break the ground for what is expected to be a challenging, exciting, and richly rewarding new field of quantum chemistry.

References

1. Kahn O (1993) *Molecular magnetism*. Wiley, New York
2. Malrieu JP, Caballol R, Calzado CJ, de Graaf C, Guihéry N (2014) *Chem Rev* 114:429–492
3. Moreira IDPR, Illas F (2006) *Phys Chem Chem Phys* 8:1645–1659
4. Neese F (2009) *Coord Chem Rev* 253:526–563
5. Illas F, Moreira IDPR, de Graaf C, Barone V (2000) *Theor Chem Acc* 104:265–272
6. Caballol R, Castell O, Illas F, Moreira IDPR, Malrieu JP (1997) *J Phys Chem A* 101:7860–7866
7. Noodleman L (1981) *J Chem Phys* 74:5737–5743
8. Noodleman L, Davidson ER (1986) *Chem Phys* 109:131–143
9. Yamaguchi K, Tsunekawa T, Toyoda Y, Fueno T (1988) *Chem Phys Lett* 143:371–376
10. Yamanaka S, Kawakami T, Nagao H, Yamaguchi K (1994) *Chem Phys Lett* 231:25–33
11. De Loth P, Cassoux P, Daudey JP, Malrieu JP (1981) *J Am Chem Soc* 103:4007–4016
12. White SR, Martin RL (1999) *J Chem Phys* 110:4127–4130
13. Schollwöck U (2011) *Ann Phys* 326:96–192
14. Moritz G, Wolf A, Reiher M (2005) *J Chem Phys* 123:184105
15. Marti KH, Ondík IM, Moritz G, Reiher M (2008) *J Chem Phys* 128:014104
16. Freitag L, Knecht S, Keller SF, Delcey MG, Aquilante F, Pedersen TB, Lindh R, Reiher M, Gonzalez L (2015) *Phys Chem Chem Phys* 17:14383–14392
17. Hu W, Chan GKL (2015) *J Chem Theory Comput* 11:3000–3009
18. Kurashige Y, Yanai T (2009) *J Chem Phys* 130:234114
19. Kurashige Y, Chan GKL, Yanai T (2013) *Nat Chem* 5:660–666
20. Sharma S, Sivalingham K, Neese F, Chan GKL (2014) *Nat Chem* 6:927–933
21. Paul S, Cox N, Pantazis DA (2017) *Inorg Chem* 56:3875–3888
22. Harris TV, Kurashige Y, Yanai T, Morokuma K (2014) *J Chem Phys* 140:054303
23. Roemelt M, Krewald V, Pantazis DA (2018) *J Chem Theory Comput* 14:166–179
24. Chan GKL, Head-Gordon M (2002) *J Chem Phys* 116:4462–4476
25. Olivares-Amaya R, Hu W, Nakatani N, Sharma S, Yang J, Chan GKL (2015) *J Chem Phys* 142:034102
26. Keller SF, Reiher M (2014) *Chimia* 68:200–203
27. Knecht S, Hedegård ED, Keller S, Kovyrshin A, Ma Y, Muolo A, Stein CJ, Reiher M (2016) *Chimia* 70:244–251
28. Bencini A, Gatteschi D (1990) *EPR of exchange coupled systems*. Springer Verlag, Berlin
29. Pantazis DA, Orio M, Petrenko T, Zein S, Bill E, Lubitz W, Messinger J, Neese F (2009) *Chem Eur J* 15:5108–5123
30. Ginsberg AP (1980) *J Am Chem Soc* 102:111–117
31. Mouesca JM, Noodleman L, Case DA, Lamotte B (1995) *Inorg Chem* 34:4347–4359
32. Noodleman L, Post D, Baerends EJ (1982) *Chem Phys* 64:159–166
33. Neese F (2004) *J Phys Chem Solids* 65:781–785
34. Dai D, Whangbo M-H (2003) *J Chem Phys* 118:29–39
35. Ruiz E, Cano J, Alvarez S, Alemany P (1999) *J Comput Chem* 20:1391–1400
36. Yamaguchi K, Takahara Y, Fueno T (1986) Ab-initio molecular orbital studies of structure and reactivity of transition metal-oxo compounds. In: Smith VH Jr, Scheaffer HF III, Morokuma K (eds) *Applied quantum chemistry*. D. Reidel, Boston, pp 155–184
37. Golub GH, Reinsch C (1970) *Numer Math* 14:403–420

38. Pantazis DA, Orio M, Petrenko T, Zein S, Lubitz W, Messinger J, Neese F (2009) *Phys Chem Chem Phys* 11:6788–6798
39. Shoji M, Koizumi K, Kitagawa Y, Kawakami T, Yamanaka S, Okumura M, Yamaguchi K (2006) *Chem Phys Lett* 432:343–347
40. Desplanches C, Ruiz E, Alvarez S (2003) *Eur J Inorg Chem* 2003:1756–1760
41. Hubner O, Fink K, Klopfer W (2007) *Phys Chem Chem Phys* 9:1911–1920
42. Coulaud E, Malrieu J-P, Guihéry N, Ferré N (2013) *J Chem Theory Comput* 9:3429–3436
43. Gutierrez L, Alzuet G, Real JA, Cano J, Borrás J, Castiñeiras A (2000) *Inorg Chem* 39:3608–3614
44. Rodríguez-Fortea A, Alemany P, Alvarez S, Ruiz E (2001) *Chem Eur J* 7:627–637
45. Pantazis DA, Krewald V, Orio M, Neese F (2010) *Dalton Trans* 39:4959–4967
46. Coulaud E, Guihéry N, Malrieu J-P, Hagebaum-Reignier D, Siri D, Ferré N (2012) *J Chem Phys* 137:114106
47. Krewald V, Neese F, Pantazis DA (2013) *J Am Chem Soc* 135:5726–5739
48. Orio M, Pantazis DA, Petrenko T, Neese F (2009) *Inorg Chem* 48:7251–7260
49. Ciofini I, Daul CA (2003) *Coord Chem Rev* 238–239:187–209
50. Bencini A, Totti F (2009) *J Chem Theory Comput* 5:144–154
51. Ruiz E (2004) *Struct Bond* 113:91–102
52. Comba P, Hausberg S, Martin B (2009) *J Phys Chem A* 113:6751–6755
53. Illas F, Moreira IDPR, Bofill JM, Filatov M (2004) *Phys Rev B* 70:132414
54. Illas F, Moreira IDPR, Bofill JM, Filatov M (2006) *Theor Chem Acc* 116:587–597
55. Zein S, Poor Kalhor M, Chibotaru LF, Chermette H (2009) *J Chem Phys* 131:224316
56. Neese F (2006) *J Biol Inorg Chem* 11:702–711
57. Amos AT, Hall GG (1961) *Proc R Soc Lond A* 263:483–493
58. Malmqvist P-Å, Roos BO (1989) *Chem Phys Lett* 155:189–194
59. Roos BO, Taylor PR, Siegbahn PEM (1980) *Chem Phys* 48:157–173
60. Andersson K, Roos BO (1992) *Chem Phys Lett* 191:507–514
61. Pierloot K, Persson BJ, Roos BO (1995) *J Phys Chem* 99:3465–3472
62. Andersson K, Malmqvist PA, Roos BO, Sadlej AJ, Wolinski K (1990) *J Phys Chem* 94:5483–5488
63. Finley J, Malmqvist P-Å, Roos BO, Serrano-Andrés L (1998) *Chem Phys Lett* 288:299–306
64. Angeli C, Cimiraaglia R, Evangelisti S, Leininger T, Malrieu JP (2001) *J Chem Phys* 114:10252–10264
65. Angeli C, Cimiraaglia R, Malrieu J-P (2002) *J Chem Phys* 117:9138–9153
66. Miralles J, Daudey JP, Caballol R (1992) *Chem Phys Lett* 198:555–562
67. Miralles J, Castell O, Caballol R, Malrieu JP (1993) *Chem Phys* 172:33–43
68. Castell O, Caballol R (1999) *Inorg Chem* 38:668–673
69. Calzado CJ, Cabrero J, Malrieu JP, Caballol R (2002) *J Chem Phys* 116:2728–2747
70. Calzado CJ, Cabrero J, Malrieu JP, Caballol R (2002) *J Chem Phys* 116:3985–4000
71. Calzado CJ, Angeli C, Taratiel D, Caballol R, Malrieu JP (2009) *J Chem Phys* 131:044327
72. Queralt N, Taratiel D, de Graaf C, Caballol R, Cimiraaglia R, Angeli C (2008) *J Comput Chem* 29:994–1003
73. Olsen J, Roos BO, Jørgensen P, Jensen HJA (1988) *J Chem Phys* 89:2185–2192
74. Malmqvist PA, Rendell A, Roos BO (1990) *J Phys Chem* 94:5477–5482
75. Ma D, Li Manni G, Gagliardi L (2011) *J Chem Phys* 135:044128
76. Li Manni G, Aquilante F, Gagliardi L (2011) *J Chem Phys* 134:034114
77. Li Manni G, Ma D, Aquilante F, Olsen J, Gagliardi L (2013) *J Chem Theory Comput* 9:3375–3384
78. Thomas RE, Sun Q, Alavi A, Booth GH (2015) *J Chem Theory Comput* 11:5316–5325
79. Li Manni G, Smart SD, Alavi A (2016) *J Chem Theory Comput* 12:1245–1258
80. Moritz G, Hess BA, Reiher M (2005) *J Chem Phys* 122:024107
81. Zgid D, Nooijen M (2008) *J Chem Phys* 128:014107
82. Chan GKL, Sharma S (2011) *Annu Rev Phys Chem* 62:465–481
83. Boguslawski K, Tecmer P, Legeza Ö, Reiher M (2012) *J Phys Chem Lett* 3:3129–3135

84. Stein CJ, Reiher M (2016) *J Chem Theory Comput* 12:1760–1771
85. Ma Y, Knecht S, Keller S, Reiher M (2017) *J Chem Theory Comput* 13:2533–2549
86. Baiardi A, Stein CJ, Barone V, Reiher M (2017) *J Chem Theory Comput* 13:3764–3777
87. Battaglia S, Keller S, Knecht S (2018) *J Chem Theory Comput* 14:2353–2369
88. Moritz G, Reiher M (2007) *J Chem Phys* 126:244109
89. Sobczak P, Barasiński A, Drzewiński A, Kamieniarz G, Klak J, Bieńko A, Mroziński J (2009) *Polyhedron* 28:1838–1841
90. Barasiński A, Sobczak P, Drzewiński A, Kamieniarz G, Bieńko A, Mroziński J, Gatteschi D (2010) *Polyhedron* 29:1485–1491
91. Schnack J, Ummethum J (2013) *Polyhedron* 66:28–33
92. Keller S, Boguslawski K, Janowski T, Reiher M, Pulay P (2015) *J Chem Phys* 142:244104
93. Sayfutyarova ER, Sun Q, Chan GK, Knizia G (2017) *J Chem Theory Comput* 13:4063–4078
94. Bao JJ, Dong SS, Gagliardi L, Truhlar DG (2018) *J Chem Theory Comput* 14:2017–2025
95. Barcza G, Legeza Ö, Marti KH, Reiher M (2011) *Phys Rev A* 83
96. Saitow M, Kurashige Y, Yanai T (2015) *J Chem Theory Comput* 11:5120–5131
97. Guo S, Watson MA, Hu W, Sun Q, Chan GKL (2016) *J Chem Theory Comput* 12:1583–1591
98. Roemelt M, Guo S, Chan GKL (2016) *J Chem Phys* 144:204113
99. Yanai T, Saitow M, Xiong XG, Chalupský J, Kurashige Y, Guo S, Sharma S (2017) *J Chem Theory Comput* 13:4829–4840
100. Boguslawski K, Tecmer P, Barcza G, Legeza Ö, Reiher M (2013) *J Chem Theory Comput* 9:2959–2973
101. Wouters S, Bogaerts T, Van Der Voort P, Van Speybroeck V, Van Neck D (2014) *J Chem Phys* 140:241103
102. Kurashige Y, Saitow M, Chalupský J, Yanai T (2014) *Phys Chem Chem Phys* 16:11988–11999
103. Chalupský J, Rokob TA, Kurashige Y, Yanai T, Solomon EI, Rulíšek L, Srnec M (2014) *J Am Chem Soc* 136:15977–15991
104. Ma Y, Knecht S, Reiher M (2017) *Chem Phys Chem* 18:384–393
105. Phung QM, Domingo A, Pierloot K (2018) *Chem Eur J* 24:5183–5190
106. Phung QM, Pierloot K (2018) *Phys Chem Chem Phys* 20:17009–17019
107. Dong G, Phung QM, Hallaert SD, Pierloot K, Ryde U (2017) *Phys Chem Chem Phys* 19:10590–10601
108. Zhang C, Chen C, Dong H, Shen JR, Dau H, Zhao J (2015) *Science* 348:690–693
109. Paul S, Neese F, Pantazis DA (2017) *Green Chem* 19:2309–2325
110. Umena Y, Kawakami K, Shen J-R, Kamiya N (2011) *Nature* 473:55–60
111. Pantazis DA, Ames W, Cox N, Lubitz W, Neese F (2012) *Angew Chem Int Ed* 51:9935–9940
112. Krewald V, Retegan M, Pantazis DA (2016) *Top Curr Chem* 371:23–48
113. Beinert H, Holm RH, Münck E (1997) *Science* 277:653–659
114. Lledós A, Moreno-Mañas M, Sodupe M, Vallribera A, Mata I, Martínez B, Molins E (2003) *Eur J Inorg Chem* 2003:4187–4194
115. Boguslawski K, Marti KH, Reiher M (2011) *J Chem Phys* 134:224101
116. Bencini A, Totti F (2008) *Inorg Chim Acta* 361:4153–4156
117. Bastardis R, Guihéry N, de Graaf C (2008) *J Chem Phys* 129:104102
118. Spivak M, Angeli C, Calzado CJ, de Graaf C (2014) *J Comput Chem* 35:1665–1671
119. Bossek U, Weyhermueller T, Wieghardt K, Nuber B, Weiss J (1990) *J Am Chem Soc* 112:6387–6388
120. Kanady JS, Tsui EY, Day MW, Agapie T (2011) *Science* 333:733–736
121. Mukherjee S, Stull JA, Yano J, Stamatatos TC, Pringouri K, Stich TA, Abboud KA, Britt RD, Yachandra VK, Christou G (2012) *Proc Natl Acad Sci USA* 109:2257–2262
122. Krewald V, Retegan M, Neese F, Lubitz W, Pantazis DA, Cox N (2016) *Inorg Chem* 55:488–501
123. Stein CJ, von Burg V, Reiher M (2016) *J Chem Theory Comput* 12:3764–3773
124. Angeli C, Calzado CJ (2012) *J Chem Phys* 137:034104
125. Bjornsson R, Lima FA, Spatzal T, Weyhermüller T, Glatzel P, Bill E, Einsle O, Neese F, DeBeer S (2014) *Chem Sci* 5:3096–3103

126. Domingo A, Specklin D, Rosa V, Mameri S, Robert V, Welter R (2014) *Eur J Inorg Chem* 2014:2552–2560
127. Kurashige Y, Yanai T (2011) *J Chem Phys* 135:094104
128. Saitow M, Kurashige Y, Yanai T (2013) *J Chem Phys* 139:044118
129. Sharma S, Chan GKL (2014) *J Chem Phys* 141:111101
130. Yanai T, Kurashige Y, Mizukami W, Chalupský J, Lan TN, Saitow M (2015) *Int J Quantum Chem* 115:283–299
131. Veis L, Antalík A, Brabec J, Neese F, Legeza Ö, Pittner J (2016) *J Phys Chem Lett* 7:4072–4078
132. Phung QM, Wouters S, Pierloot K (2016) *J Chem Theory Comput* 12:4352–4361